OPEN ACCESS

GAVIN PUBLISHERS

Journal of Community Medicine & Public Health

Research Article

Moukoko D, et al. J Community Med Public Health 4: 177.
DOI: 10.29011/2577-2228.100077

Distinct Articular and Endochondral Differentiation Pathways in Bone Marrow Chondrogenic Progenitor Cells

D. Moukoko[1], M. Pithioux[2-4*], F. Roseren[2-4], D. Pourquier[5]

[1]Pediatric Orthopaedic Surgery Department, Angers, CHU, Angers, France

[2]Aix Marseille University, CNRS, ISM, Marseille, France

[3]Aix Marseille University, APHM, CNRS, ISM, Sainte-Marguerite Hospital, Institute for Locomotion, Department of Orthopaedics and Traumatology, Marseille, France

[4]Aix Marseille University, CNRS, ISM, Anatomic laboratory, Timone, Marseille, France

[5]Pathology Department, Institut régional du Cancer de Montpellier (ICM)-Val d'Aurelle, Montpellier, France

[*]**Corresponding author:** M. Pithioux, Department of Orthopedics and Traumatology, Aix Marseille University, Marseille Public University Hospital System (APHM), French National Center for Scientific Research (CNRS), Institute of Movement Science (ISM), Sainte Marguerite Hospital, IML, Marseille, France

Citation: Moukoko D, Pithioux M, Roseren F, Pourquier D (2020) Distinct Articular and Endochondral Differentiation Pathways in Bone Marrow Chondrogenic Progenitor Cells. J Community Med Public Health 4: 177. DOI: 10.29011/2577-2228.100077

Received Date: 11 March, 2020; **Accepted Date:** 27 March, 2020; **Published Date:** 02 April, 2020

Abstract

Bone marrow contains skeletal progenitor cells (mesenchymal stem cells) which are important actors in skeletal repair. Nevertheless, the therapeutic use of mesenchymal stem cells for articular cartilage repair remains a challenge with a limited efficacy on both clinical outcomes and cartilage regeneration. In rabbit periosteal graft models, we show that such skeletal progenitor cells are recruited and undergo differentiation through different skeletal tissue pathways (bone, cartilage, skeletal muscle) in bone marrow areas that are under periosteal graft influence. Moreover, histological observations show among cartilage differentiated cells two different cartilage pathways, corresponding respectively to articular cartilage formations and to endochondral cartilage formations. This underline the presence in bone marrow of cartilage progenitor cells that escape from the intrinsic endochondral differentiation program resulting in transient rather than permanent cartilage, and follow a specific articular cartilage differentiation pathway. With respect to tissue engineering, and while extremely complex techniques are being developed to artificially generate functionally integrated, stratified articular cartilage like structures, our observations urge the development of protocols that select the proper population of articular cartilage progenitor cells before its use as cartilage building units.

Keywords: Articular cartilage repair; Tissue engineering; Skeletal progenitors; Mesenchymal stem cells; Articular cartilage pathway; Endochondral cartilage pathway; Periosteum

Introduction

Bone marrow contains skeletal progenitor cells (also referred to as bone marrow mesenchymal stem cells [bone marrow MSCs] or bone marrow stromal cells) which are multipotent cells making them prime candidates for bone and articular cartilage repair [1,2]. The periosteum is a membrane covering the external surface of long bones and it plays a major role in skeletal repair [3,4] and contains skeletal stem cells with high bone regenerative potential [5]. Moreover, periosteal grafts have been shown to have osteochondrogenic potential because they induce the formation of osteocartilaginous tissue neoformations at their site of implantation [6,7]. When a periosteal graft is transferred to an ectopic site, a new bone tissue is produced through the proliferation and differentiation of mesenchymal progenitor cells derived from the periosteum, but also from the surrounding host tissues [8]. The local mechanical environment is also known to affect the differentiation pathway adopted by mesenchymal progenitors to produce bone, cartilage or fibrous tissue during skeletal tissue repair, which is the basis of the field of mechanobiology [9]. The aim of a first study carried out by our team and focusing on mechanobiology [10] was to investigate the sequence of histological events that occur within the area of transplanted periosteum following periosteal grafting, under environmental conditions of mechanical loading compared to conditions of immobility in a rabbit model. In a first group of rabbits a periosteal flap was implanted in the calf muscle and tissue

neoformation occurred in the absence of specific mechanical loading (muscular model/control group). In a second group the tissue neoformation process was subjected to mechanical loading by the proximity of the graft with the knee joint (articular model/loaded group). Our observations showed osteocartilaginous neoproduction at the site of implantation of the periosteal grafts in both groups (Figure 1).

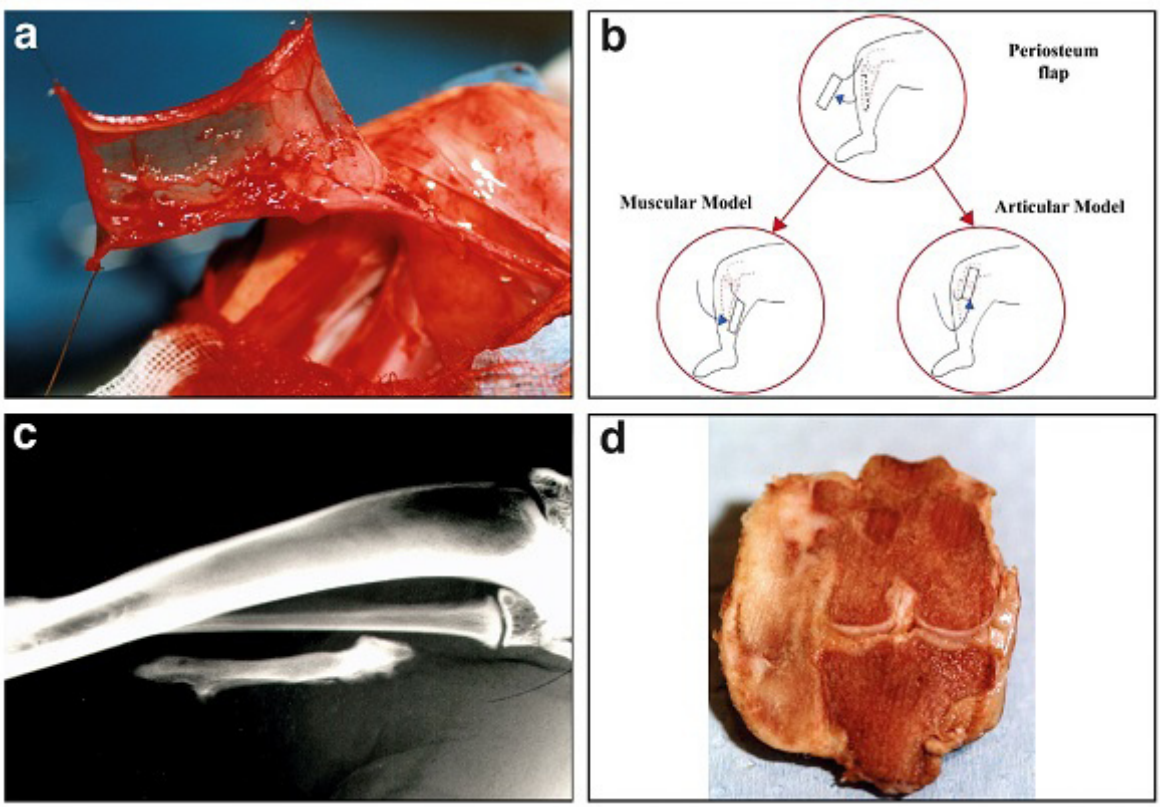

Figure 1: The two models of periosteum graft. **A.** Surgical removal of the periosteum graft taken from the anterior surface of the tibia. The graft resembles a fine vascularised membrane. The vascular pedicle is visible on the right. **B.** Diagram of the two models: harvested periosteum grafts are implanted in the calf muscle (muscular model) or beside the knee in a para-articular position (articular model). **C.** Muscular model on D60, X-ray view showing a bone neoformation in calf muscle. **D.** Articular model, macroscopic view following section in the frontal plane of a D45 observation, presence of a large bone neoformation on the medial side of the knee joint, bridging the femur and tibia.

Histologically the neoproduction followed an endochondral ossification-like sequence, i.e. a process of bone formation beginning with the constitution of a cartilage anlage, followed by the formation of an ossification front resulting in the creation of bone, then followed by remodeling of the bone with the formation of a medulla. In the articular model, development was affected by mechanical constraints related to the proximity of the graft with the knee joint. These observations complied with findings in mechanobiology.

Nevertheless, other important observations were realized in tissues adjacent to periosteum graft implantation site, in the two models. It consisted in the presence of bone, cartilage and skeletal muscle cells collections in the femur and tibia bone marrow, the knee joint cavity and adjacent skeletal muscles. Brief observations on these cell collections were presented in this first work. The present work focuses the distribution of these cell collections within bone marrow and other tissues and details of the various articular phenotypes that are observed. Different sub-types of cartilage are characterized through histological observation of undecalcified methylmethacrylate embedded samples.

Methods

Animal model

Three month-old male New Zealand rabbits weighing 2.5

kg (animal source/Institut National de Recherche Agronomique [INRA] Montpellier, France were used as animal model. Seventeen rabbits underwent surgery on both hind legs at once, the left leg was used for the articular model, and the right leg for the muscular model. Observations were made at 8 time points using 2 animals on day four (D4), 2 on D7, 3 on D15, 2 on D30, 2 on D45, 2 on D60, 2 on D90, and 2 on D180. All experiments were performed in the Experimental Surgery Laboratory of Montpellier Academic Medical School and were approved by the institutional board in accordance with French guidelines on experimental animal studies.

Surgical procedures

Rabbits were anesthetized with acepromazine (Vetranquil 1%/Ceva) intravenous injection and then a mixture of xylazine (Rompun 2%/Bayer) and ketamine (Imalgene 500/Merial) intravenous injection.

Harvesting of the periosteal flaps

In both models, the skin was incised longitudinally on the medial surface of the legs under strict aseptic conditions. The tibialis anterior muscle was exposed subcutaneously. Its fascia was cut along its insertion on the periosteum of the tibia anterior crest. The muscle body was lifted away from the tibia, exposing the lateral surface of the bone. The periosteum was incised longitudinally on the lateral surface of the tibia diaphysis and a flap measuring 30 mm in length and 10 mm in width was lifted towards the postero-medial tibia crest. The periosteal flap was freed from any attachment to muscle tissue. It was vascularized by the saphenous vascular bundle, via superficial fascial attachments.

Muscular model

In the first group of animals corresponding to the control group, referred to as the "muscular model", tissue neoformation occurred in the absence of specific mechanical loading. In this model, the harvested periosteal was implanted in the right calf muscle. In this group, the periosteal flap was sutured onto the medial gastrocnemius muscle which provided support, with its cambium layer facing the muscle fascia.

Articular model

In a second group corresponding to the loaded group, referred to as the "articular model", the tissue neoformation process was subjected to mechanical loading by the proximity of the graft with the knee joint. In this group, the harvested periosteal flap was attached to the medial side of the left knee joint, bridging the tibia and the femur. The proximal edge was sutured to the distal part of the femur and the distal edge to the tibia, so that its middle part bridged the joint line. The cambium layer was directed towards the joint. While suturing the graft, great care was taken not to penetrate the articular capsule.

Periosteum graft and semi-permeable filter

In two animal's left leg, a periosteal graft harvested in the same way was directly positioned on the tibia surface with interposition of a semi-permeable filter (Polycarbonate PCTE membrane filter/ Sterlitech Inc) with 0.4 µm diameter pores between bone surface and graft. The animal was sacrificed on D30.

Post-operative period

After surgery, the rabbits where allowed to move around spontaneously outside their cage for one hour per day, otherwise movement was limited to the cage.

Sacrifice and macroscopic examination

After the prescribed time, each animal was sacrificed with a pentobarbital (EuthasolVet/TVM) intravenous injection. After sacrifice, gross examination of the field of surgery was carried out and tissues were sampled and fixed for histology. The samples taken for observation in the articular model were adapted on a case by case basis. The specimens were withdrawn taking into account the position of the longitudinal axis of the neoformation as observed macroscopically. The position of the longitudinal axis varied significantly from one observation to another which explains why the corresponding histological specimens were prepared either in the frontal plane or in the sagittal plane of the knee, depending on the observation.

Radiological controls

Radiological controls of samples were performed on a 500 T Senix H.F Mammograph (General Electric/CGR).

Histology

Histological slides were mainly prepared using undecalcified methyl methacrylate-embedded samples fixed with 70% ethanol. After fixation, samples were dehydrated in an ethanol 100% bath, then ethanol was substituted with methylcyclohexan (Elvetec Services), then samples were impregnated with methyl methacrylate (Merck) at 4°C temperature, then embedded in methyl methacrylate at 32°C temperature. Ten µm-thick sections were cut with a microtome Polycut (Reichert Jung). Three different stainings were used, May-Grünwald-Giemsa (MGG), Goldner's Trichroma (Trichroma) and Solochrome Cyanin R (Solochrome).

Staining procedures

For May-Grünwald-Giemsa stain, sections were immersed successively in May-Grunwald dye (Merck) during 15 minutes at 37°C temperature, then in Giemsa dye (Merck) during 45 minutes at 37°C temperature, then rinsed with tap water. At the end sections were dehydrated in absolute ethanol and mounted between the two glass slides with the mounting medium Neo Entellan (Merck). For the Goldner' s Trichrome stain, sections were immersed

successively in Weigert's Hematoxylin dye (Merck) during 10 minutes at room temperature, then in Fuchsin Ponceau dye (Merck) during 5 minutes at room temperature, then in Molybdic orange G 6 dye (Merck) during minutes at room temperature, then in Light green dye (Fluka) during 5 minutes at room temperature. Between each dye, sections were rinsed with tap water. At the end, sections were dehydrated and mounted in the same way than for May-Grünwald-Giemsa stain. For Solochrome Cyanin R stain, sections were immersed in Solochrome Cyanin R dye (BDH Prolabo) during 30 minutes at room temperature, then rinsed in tap water. Dehydration and mounting were realized in the same way as for May-Grünwald-Giemsa stain. Some histological slides were prepared with formaldehyde fixed, undecalcified or decalcified, paraffin-embedded samples and then cut in three µm-thick sections and stained with Hematein-Eosin-Saffron (HES) stains.

Light microscopy observations and photographs of histologic preparations were performed using an Olympus BX50 light microscope + Olympus E 620 digital camera. For very low power views of histologic preparations, the slides were directly photographed on a light table with a Canon reflex camera + Sigma 105 mm macro lens.

Results

Muscular model

At the time of sacrifice in the early stage (D4) following grafting, the implantation site was found to be edematous in appearance on macroscopic observation. At later stages, dissection of the soft tissues revealed longitudinal cartilage/bone formations ranging from 2.7 cm to 3.2 cm in length and X-rays confirmed the presence of bone. At the D4 stage, histological analysis of the periosteal graft region revealed a tissue resembling a blastema containing a densely packed population of spindle-shaped mononuclear cells. In the underlying skeletal muscle, a band of muscle necrosis of uniform thickness had developed beneath the periosteal graft with a regenerative area deeper in the muscle containing numerous blastic cells within a well defined layer. At the D7 stage, a cartilaginous anlage including an ossification front was observed. This newly formed tissue was composed of approximately 50% bone and 50% cartilage. Almost complete muscle regeneration was observed at the same time. Subsequently (D15), the cartilage was very largely replaced by bone. In the later observations (D30 to D180), the neoformed bone structures were sometimes associated with a medullary cavity containing bone marrow. Areas of fibrous differentiation continuous with the bone structures were also observed (Figure 2).

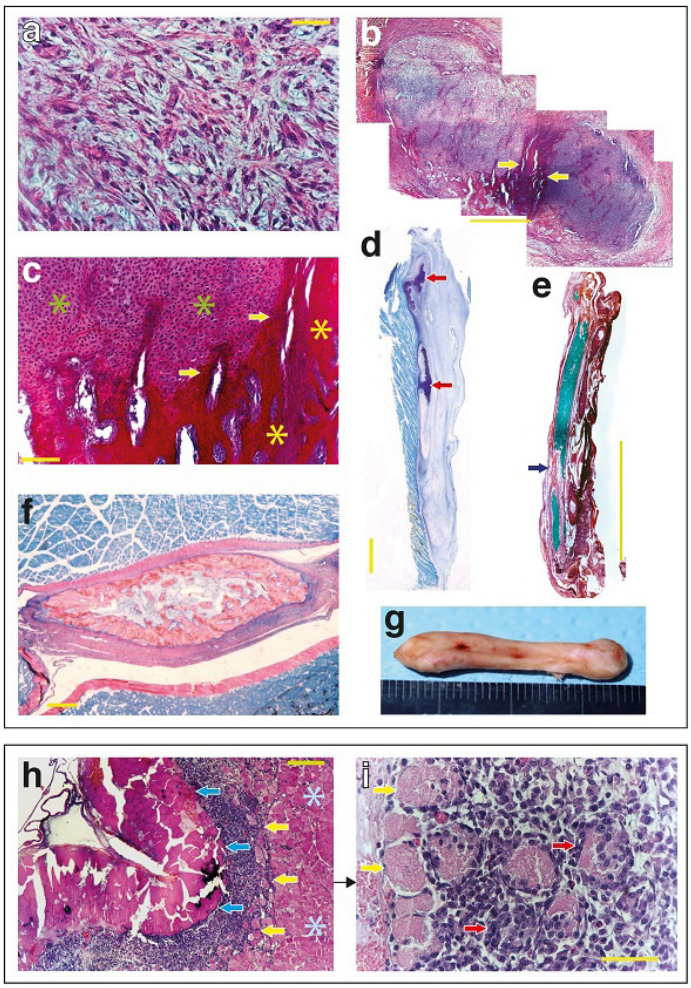

Figure 2: Muscular model: bone neoformation process and adjacent muscle necrosis. **A.** Periosteal graft area on D4, a densely packed population of spindle-shaped cells constitutive of an immature blastema is visible (HES, Scale bar 40 µm). **B.** Cartilaginous anlage and ossification front (arrows) on D7 (HES, Scale bar 1.3 mm). **C.** Higher power view of ossification front (arrows) (HES, Scale bar 150 µm). **D.** View of neoformation on D15, large areas of cartilage are visible (arrows) (MGG, Scale bar 2.5 mm). **E.** Bone neoformation on D60 showing compact bone formation and an area of focal fibrous differentiation (arrow) (Trichroma, Scale bar 13.3 mm). **F.** Transversal section of bone neoformation showing a medullary cavity containing bone marrow on D30 (MGG, Scale bar 500 µm). **G.** Macroscopic view of a bone formation on D 45. **H.** Skeletal muscle necrosis underneath the periosteal graft on D4: intact muscle (stars), with a regenerative area (yellow arrows) of uniform thickness and under a necrotic area of uniform thickness (blue arrows) (HES, Scale bar 400 µm). **I.** High power view of the regenerative area with necrotic fibers (yellow arrows) and numerous myoblasts in and around regenerating fibers (red arrows) (HES, Scale bar 60 µm).

Additionally, in two of the seventeen muscular model observations (D15 and D30 observations), bone, cartilage and skeletal muscle cells collections were noted in some sectors of the tibia bone marrow and in the intermuscular septa of adjacent skeletal muscles (Figure 3).

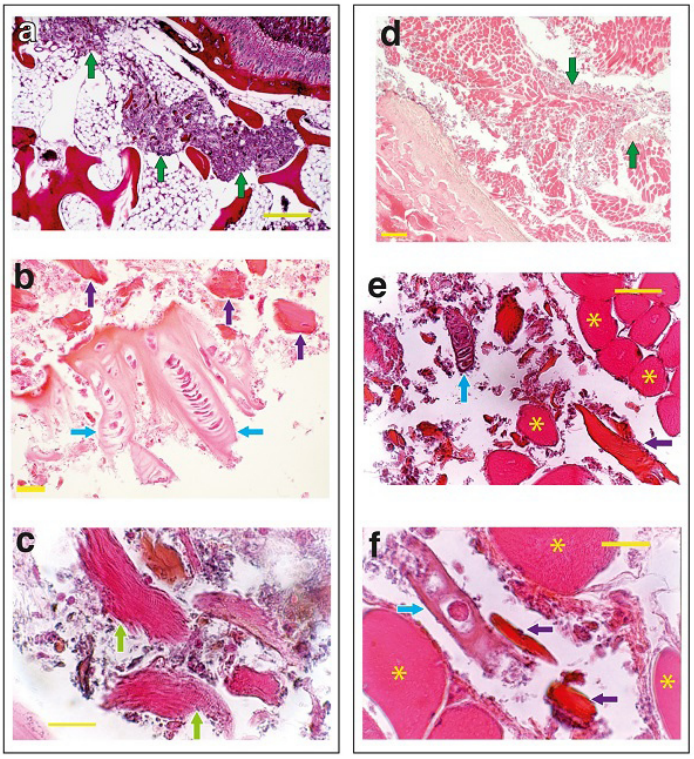

Figure 3: Muscular model, bone marrow and intramuscular cells collections. **A.** Bone marrow cells collections on D30 muscular model (arrows) (HES, Scale bar 200 µm). **B.** High power view of cartilage formations (blue arrows) and bone formations (violet arrows) (HES, Scale bar 10 µm). **C.** High power view of skeletal muscle formations (arrows) (HES Scale bar 20 µm). **D.** Intramuscular cells collections on D15 muscular model (arrows) (HES, Scale bar 300 µm). **E.** High power view of cartilage formations (blue arrow), bone cells formations (violet arrows) and native muscle fibers (stars) (HES, Scale bar 50 µm). **F** Very high power view of cartilage formations (blue arrow) and bone cells formations (violet arrows) and native muscle fibers (stars) (HES, Scale bar 20 µm).

Figure 4 shows a simplified diagram of the sequence of events that occurred in the muscular model.

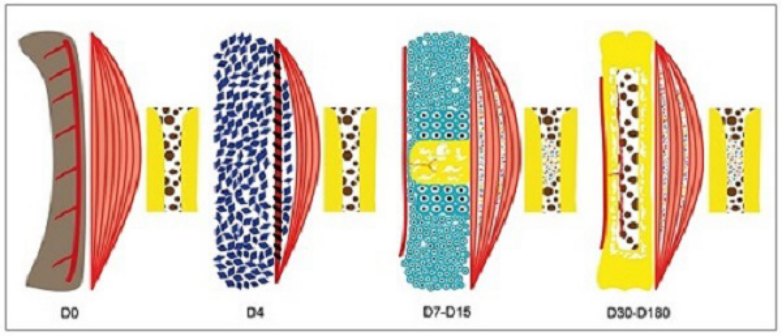

Figure 4: Diagram of the sequence of events in the muscular model. **Step 1 (D0):** Periosteum graft implanted in the muscle. **Step 2 (D4):** Immature blastema in the area of the graft, process of muscle necrosis/regeneration in the muscle area in contact with the graft (shaded area). **Step 3 (D7 and D15):** Formation of a cartilaginous anlage, endochondral ossification, healing of the muscle, cells collections in muscle and in tibia bone marrow. **Step 4 (D30 to D180):** Neoformation entirely made up of bone with formation of a medullary cavity, cells collections in muscle and in tibia bone marrow.

Articular model

In the articular model, new bone was formed on the lateral side of the knee joint on macroscopic observation (Figure 1C) and histology confirmed the development of a tissue structure on the medial side of the knee joint, bridging the femur and tibia. The neoformation developed according to the same sequence as in the muscular model, but the volume of the newly formed bone was nevertheless extremely variable between observations with the neoformation sometimes being composed solely of simple fibrous tissue. In several observations, cartilage persisted beyond D15 in some areas (the latest time point at which cartilage was observed in the neoformations in the muscular model) up to D45. Additionally, in some observations, we noted large areas of cartilaginous tissue with "confrontation" of cartilaginous masses.

At later time points (D60 to D180), however, all observations showed complete ossification associated with areas of fibrous differentiation. Inside bone neoformation a medullary cavity could be seen. In several observations, the neoformed bone was found to be continuous with native tibia bone.

In different samples, we identified bone, cartilage, skeletal muscle cells collections intimately mixed. The vast majority (about 90%) of cells in these collections were bone cells. These cells were found beneath the neoformation in the joint cavity of the knee, in intermuscular septa in the surrounding skeletal muscles, in areas of the tibia and femur bone marrow, in endosteum and "lifting" the periosteum. The cells were observed from D4 and were still present at D180 but their abundance and distribution varied considerably between observations.

They were absent in some tissues while present in others, for example absent in the bone marrow and present in the joint cavity (Figures 5-8).

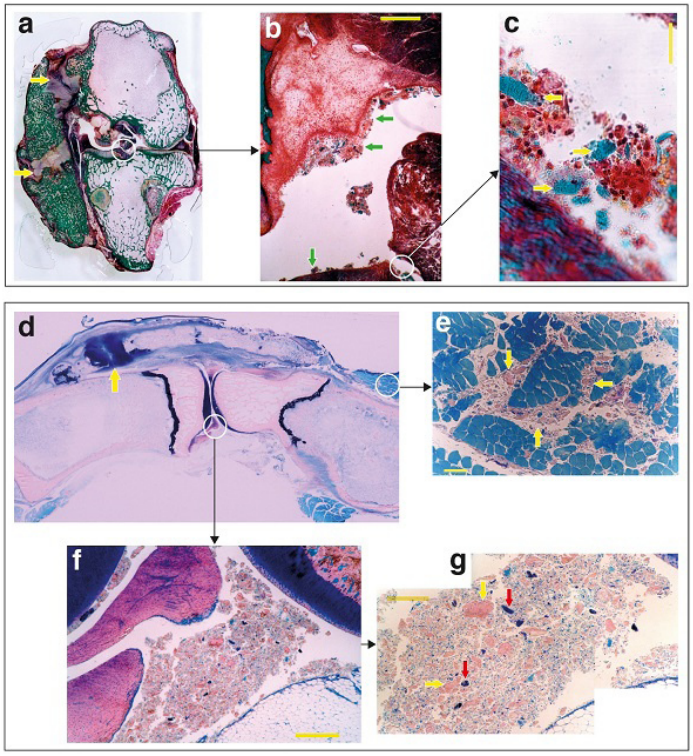

Figure 5: Articular models. **A.** Large view of an articular model sample on D45, osteocartilaginous neoformation having developed on contact with the knee is visible. Cartilaginous areas are visible (arrows), focus on intra-articular cells collections (Trichroma). **B.** Higher view centered on intra-articular cells collections (arrows) (Scale bar 400 µm). **C.** Very high power view of this area, the arrows show bone cells (Scale bar 40 µm). **D.** Large view of an articular model on D15, presence of a large bone neoformation with an area showing cartilaginous area (arrow), foci on intra-articular and intramuscular cells collections (MGG). **E.** Cells collections in adjacent muscle (arrows) (Scale bar 100 µm). **F.** View centered on the knee joint showing the presence of intra-articular cells (Scale bar 400 µm). **G.** High power view of intra-articular cells, numerous bone cells (yellow arrows) and altered cartilaginous cells are visible (red arrows) (Scale bar 200 µm).

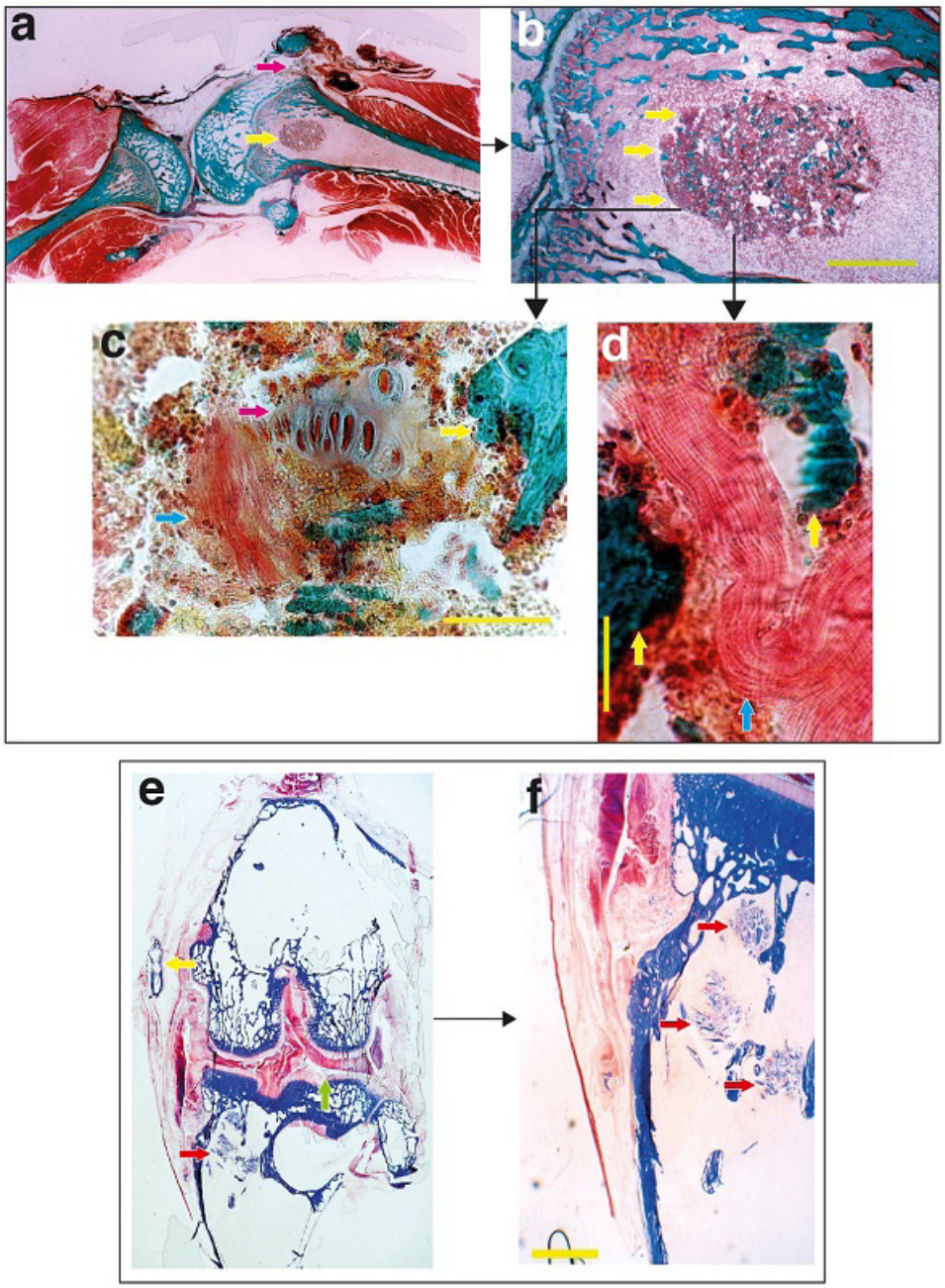

Figure 6: Articular models. **A.** Articular model on D30, fibrous neoformation in the anterior part, intra-articular cells collections (pink arrow), intramedullary area of cells collections in femur bone marrow (yellow arrow) (Trichroma). **B.** Focus on cells collections in femur bone marrow (arrows) (Scale 2 mm). **C.** High power view showing bone cells (yellow arrow), cartilage cells (pink arrow) and skeletal striated muscle cells (blue arrow) (Scale bar 30 µm). **D.** High power view showing bone cells (yellow arrows) and striated skeletal muscle cell (blue arrow) (Scale bar 30 µm). **E.** Articular model on D180, presence of a bony and fibrous neoformation in contact on the lateral side of the knee with a medullary cavity within the bony neoformation (yellow arrow). Intramedullary cells collections in tibia (red arrow) and intra-articular cells collections (green arrow) (Solochrome). **F.** View centered on the intramedullary cells collections in the tibia (arrows) (Scale bar 2 mm).

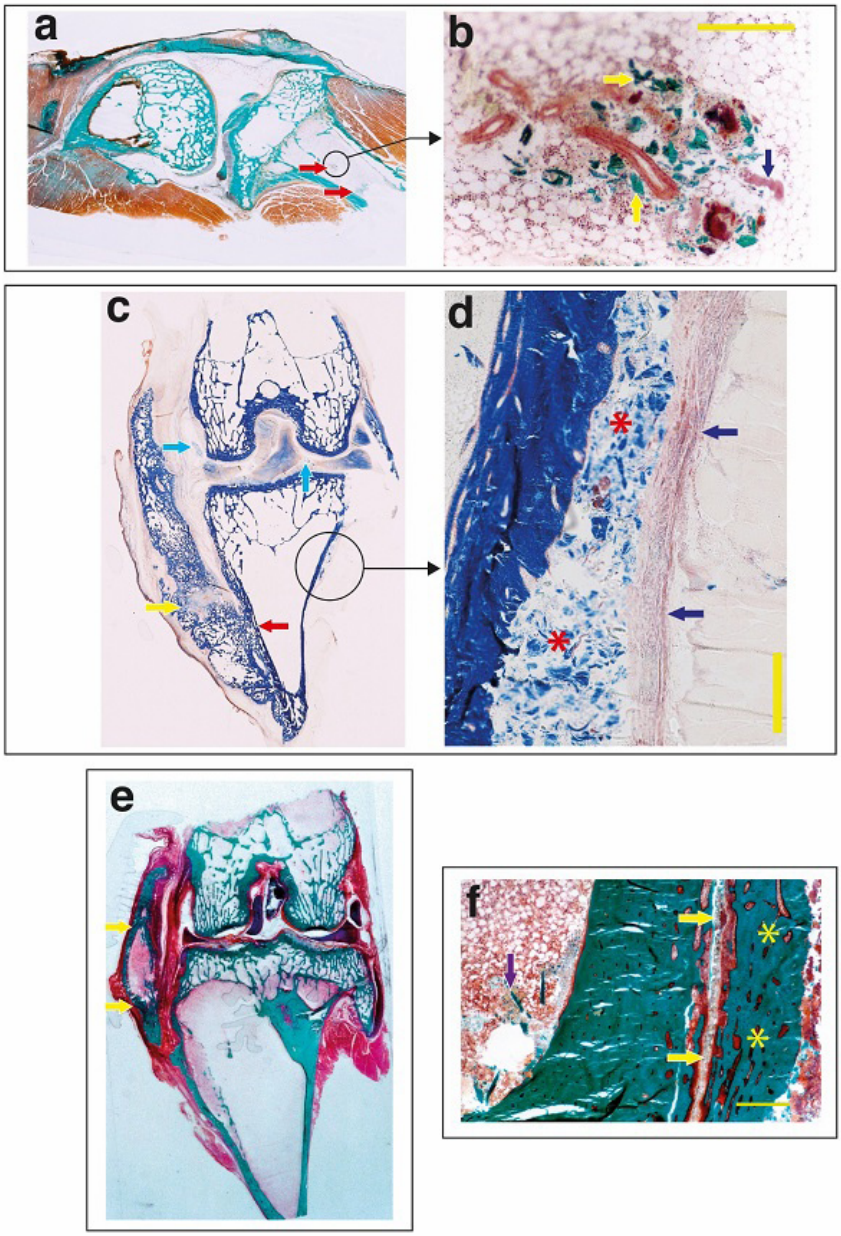

Figure 7: Articular models + semipermeable membrane test. **A.** Large view of an articular model on D60, fibro/osseous neoformation in the anterior part, littles areas of cells collections in femur bone marrow (arrows) (Trichroma). **B.** View centered on one of the cells collection, with bone cells (yellow arrows) and skeletal muscle cells (blue arrow) (Scale bar 300 µm). **C.** Large view of an articular model on D45, large osteocartilaginous neoformation in contact with the knee with merging of the newly formed bone with the native tibial bone (red arrow), a cartilaginous area can be seen on the neoformation (yellow arrow), intra-articular cells collections (blue arrows), focus on cells collections "lifting" the periosteum of the tibia (Solochrome). **D.** View centered on cells collection (red stars) "lifting" the periosteum (arrows) (Scale bar 300 µm). **E.** Large view of an articular model on D 90 large osseous on the lateral side of the knee with a medullary cavity formed into new formed bone (arrows) (Trichroma). **F.** Periosteal flap directly repositioned on the tibia with a semipermeable filter (confer discussion): bone neoformation (stars), semipermeable filter (yellow arrows), cells collections in tibia bone marrow (violet arrow) (Trichroma, Scale bar 500 µm).

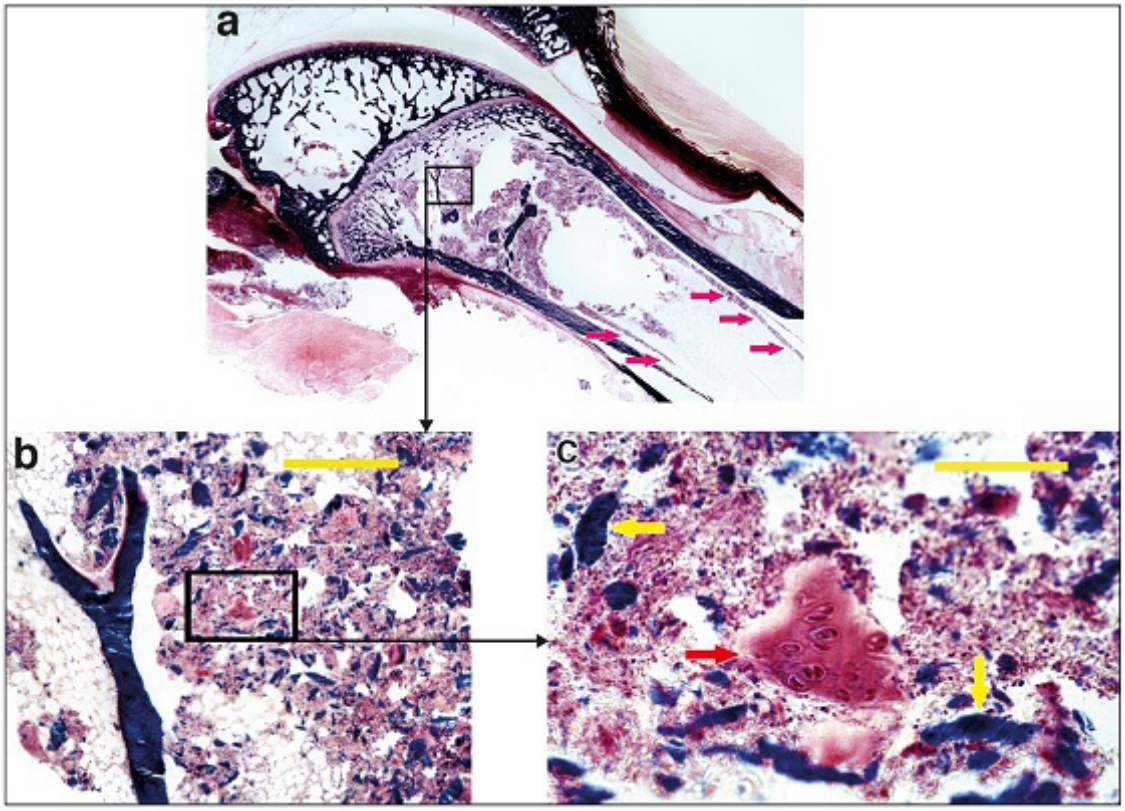

Figure 8: Articular model. **A.** Articular model on D30, extensive cells collections in distal femur bone marrow, cells collections in femur endosteum (arrows) (Solochrome). **B.** View centered on bone marrow cells collections (Scale bar 500 µm). **C.** High power view showing cartilage cells formation (red arrow) and bone cells formations (yellow arrows) (Scale bar 50 µm).

In joint spaces and intermuscular septa cartilage cells showed signs of cell injury (Figure 5G). These cells were usually scarce and present in small clusters in bone marrow. They were nevertheless present in great quantities in one observation (see Chapter**:** Two types of cartilage in bone marrow collections).

Twelve of the seventeen articular model observations included cell collections of diverse density.

D4 stage in articular

The D4 stage observation should be described in detail. At this stage, the implantation zone of the graft was made up of immature cells. We also noted numerous immature and mitotic cells in large areas in the bone marrow. Bone and cartilage cells collections were identified in the joint cavities and in adjacent muscles. Moreover, intense osteoclastic/osteoblastic activity, providing evidence of bone remodeling, was observed in the tibia and femur bones beneath the periosteal flap. Skeletal muscles adjacent to the periosteal graft showed areas of necrosis (Figure 9).

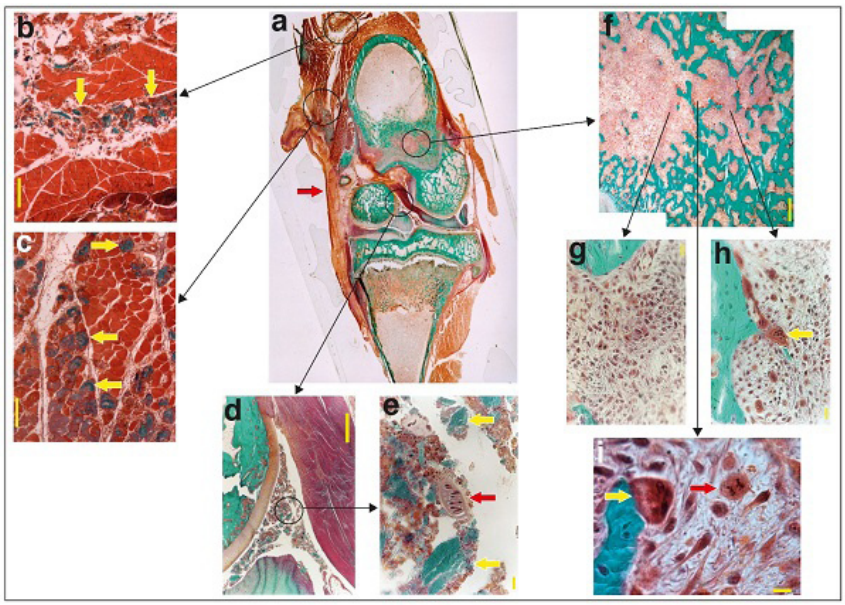

Figure 9: Articular model on D4. **A.** Large view of an articular model on D4: periosteum graft area (arrow) (Trichroma). **B.** Intramuscular cells collections (arrows) (Scale bar 200 µm). **C.** Muscle fiber necrosis in skeletal muscle adjacent to graft (arrows) (Scale bar 200 µm). **D.** Intra-articular cells collections (arrows) (Scale bar 500 µm). **E.** High power view on intra-articular cells collections with a cartilage cells formation (red arrow) and bone cells formations (yellow arrows) (Scale bar 20 µm). **F.** Immature cells area in femur bone marrow (Scale bar 400 µm). **G.** High power view on immature cells (Scale bar 20 µm). **H.** Bone remodeling in the femur bone with osteoclasts (arrow) (Scale bar 20 µm). **I.** High power view showing an osteoclast (yellow arrow) and immatures cells with a mitotic figure (red arrow) (Scale bar 10µm).

Figure 10 shows a simplified diagram of the sequence of events that occurred in the articular model.

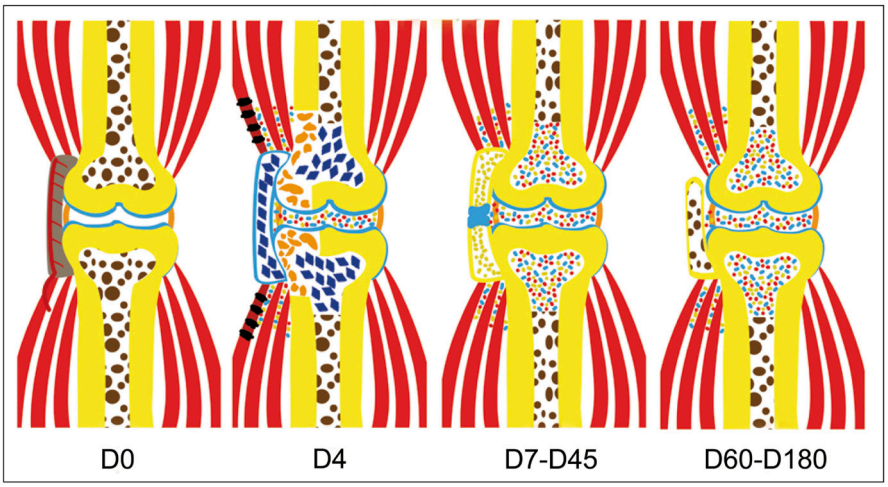

Figure 10: Diagram of the sequence of events in the articular model. **Step 1 (D0):** Periosteum graft implant bridging the knee. **Step 2 (D4):** Immature blastema in the area of the graft and immatures cells in bone marrow, presence of intra-articular and intramuscular cells collections. Bone remodeling (orange areas) and muscle necrosis (shaded areas). **Step 3 (D7 to D45):** Osteocartilaginous neoformation bridging the knee with persistence of cartilaginous areas up to D45, presence of intramedullary, intra-articular and intramuscular cells collections, muscle healing. **Step 4 (D60 to D180):** Bone neoformation entirely consisting of bone and formation of a medullary cavity, persistence cells collections.

Two types of cartilage in bone marrow collections

In one specific observation corresponding to Figure 8 sample (D30), well-preserved, cell-rich collections were seen in bone marrow. High power examination of these cells collections in different section levels and using different stains showed different features in cartilaginous and osteocartilaginous formations. Some images were very evocative of the columns of cartilage cells observed during the process of endochondral ossification of the epiphyseal plate (growth plate), showing piles of cells associated at their extremities with hypertrophic cells. These two aspects correspond respectively to the proliferative and hypertrophic zones of the cartilage epiphyseal plate. Some of the cell columns also included a bony component continuous with the cartilaginous cells and resembling an ossification front. Other cartilage formations were found to have a typical articular cartilage morphology with radial (deep), transitional (middle) and tangential (superficial) layers. Some of these articular cartilage formations also showed a bony component, apparently corresponding to subchondral bone. Formations with histological features allowing clear characterization as either articular or endochondral cartilage were found in small numbers. Such very specific characterization was only possible if the observed cartilaginous formation was particularly favorably orientated with respect to the plane of the section. However, with careful examination, all the cartilaginous formations observed could *a priori* be classified as either articular cartilage or endochondral cartilage. Quantitatively, articular and endochondral cartilage formations were distributed approximately in an equitable proportion (Figures 11-15).

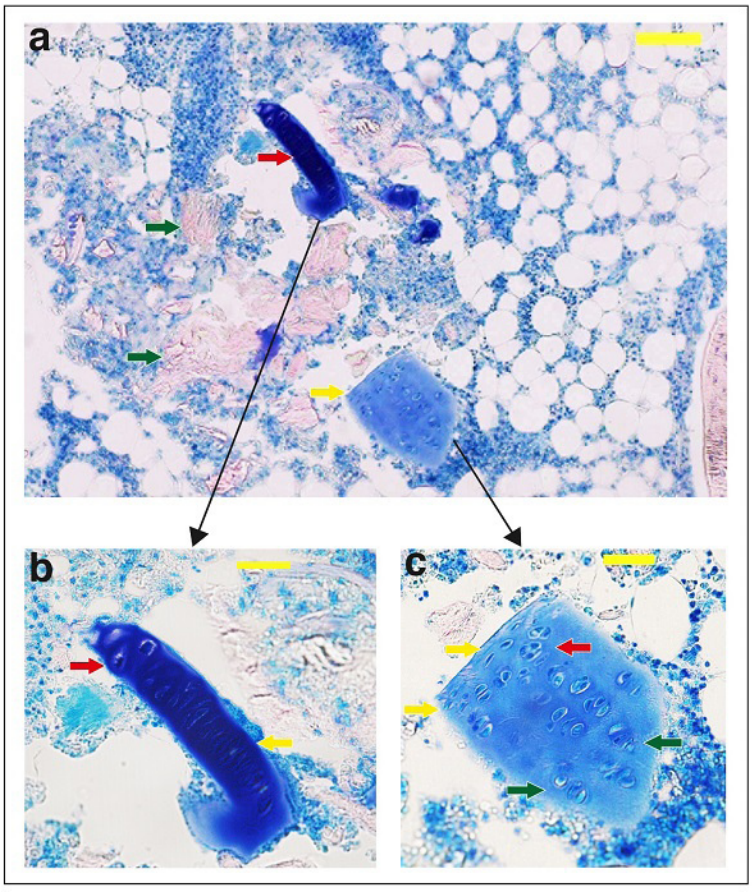

Figure 11: Two types of cartilage formations in bone marrow (MGG stain). A. In bone marrow, cells formations comprising, articular cartilage (yellow arrow), endochondral cartilage (red arrow) and bone (green arrows) formations (Scale bar 100 µm). **B.** High power view on the endochondral cartilage formation, proliferative area (yellow arrow) and hypertrophic cells area (red arrow) (Scale bar 40 µm). **C.** High power view on the articular cartilage formation with the tangential (yellow arrows), transitional (red arrow) and radial (green arrows) layers (Scale bar 40 µm).

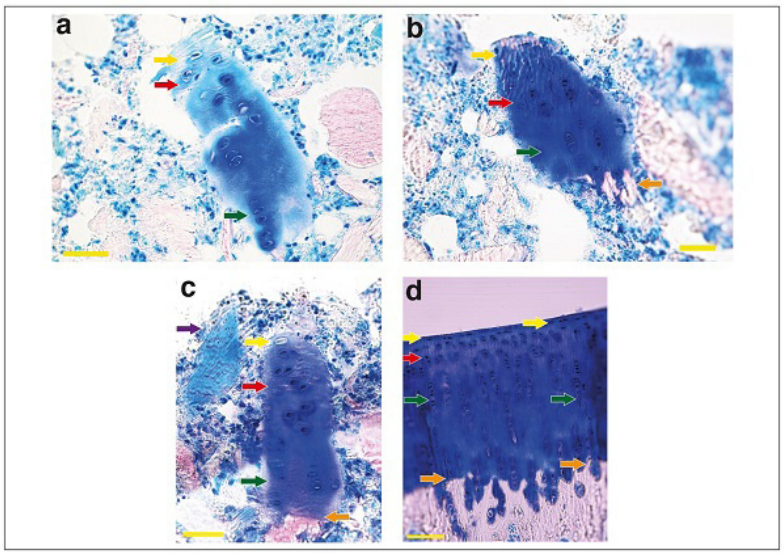

Figure 12: Articular cartilage formations in bone marrow (MGG stain). **A.** Articular cartilage formation with the tangential (yellow arrow), transitional (red arrow) and radial (green arrow) layers (Scale bar 40 µm). **B.** Articular osteochondral formation with tangential (yellow arrow), transitional (red arrow), radial (green arrow) layers and cartilage/subchondral bone junction (orange arrow) (Scale bar 50 µm). **C.** Articular osteochondral formation with, tangential (yellow arrow), transitional (red arrow) and radial (green arrow) layers, cartilage/subchondral bone junction (orange arrow) and muscle cells formation (violet arrow) (Scale bar 40 µm). **D.** For comparison with figures A, B, C view of the native articular cartilage and subchondral bone showing tangential (yellow arrows), transitional (red arrow), radial (green arrows) layers and the cartilage/subchondral junction (orange arrow) (Scale bar 60 µm).

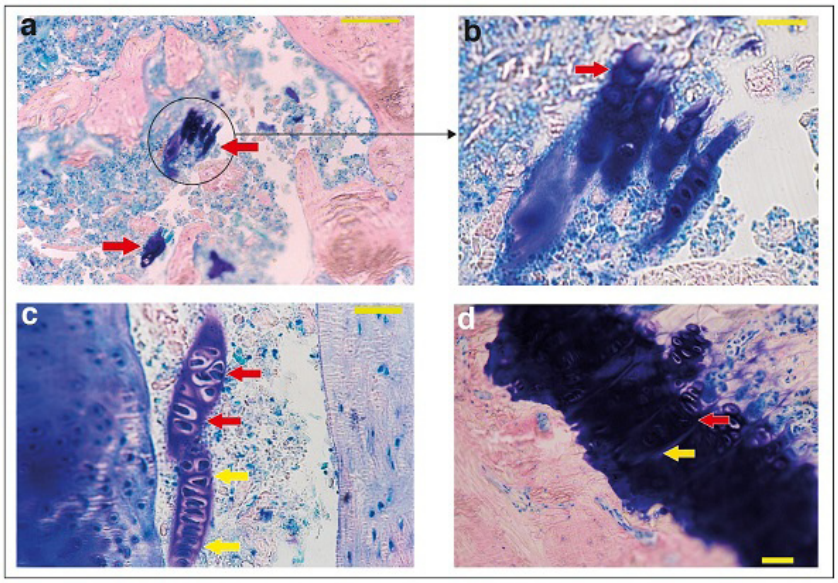

Figure 13: Endochondral cartilage formations in bone marrow and intra-articular (MGG stain). **A.** View of endochondral cartilage formations (arrows) in bone marrow (Scale bar 200 µm). **B.** High power view of one formation, comprising four cells columns, hypertrophic cells are visible (arrow) (Scale bar 50 µm). **C.** Intra-articular endochondral formations, two columns of cartilage cells are observed, first column with hypertrophic cells (red arrows), second column with hypertrophic and proliferative cells (yellow arrows) (Scale bar 100 µm). **D.** For comparison with figures A, B, C, view of the native growth plate in the same sample comprising columns of cartilaginous cells with proliferative area (red arrow) and area of hypertrophic cells (yellow arrow) (Scale bar 50 µm).

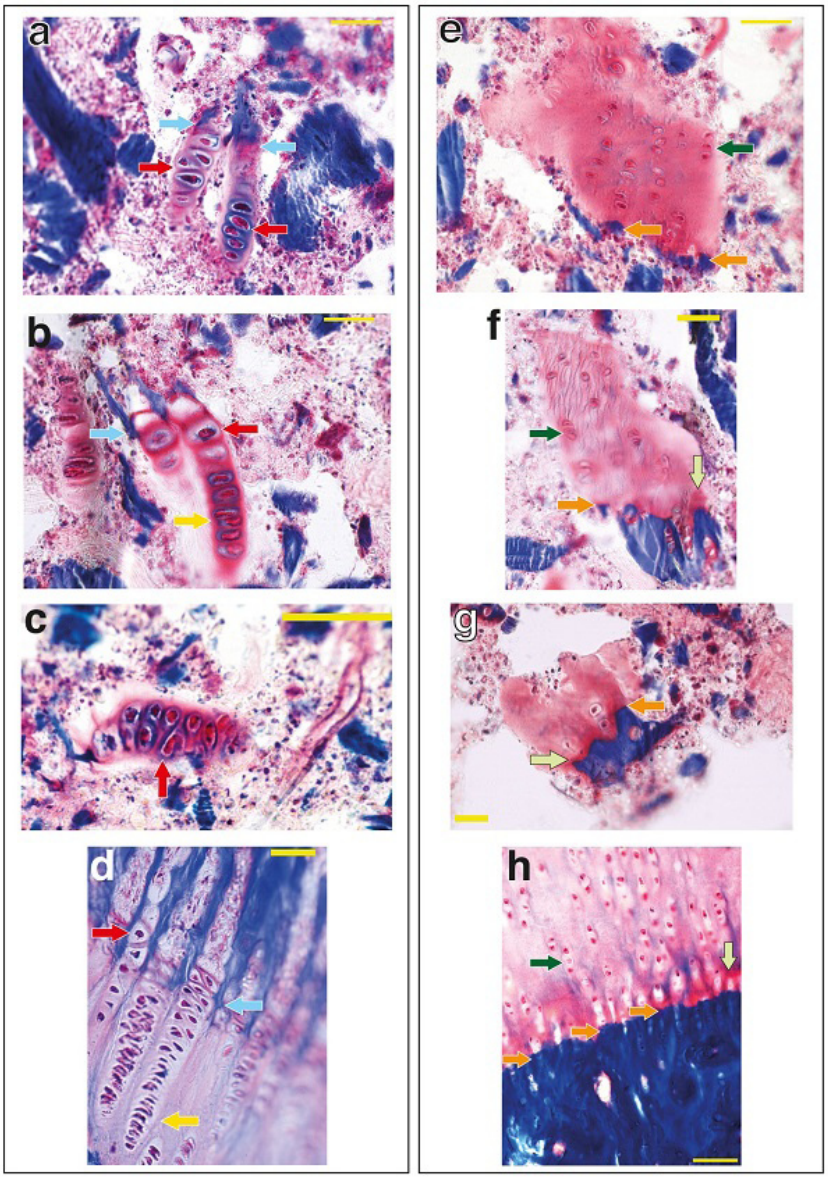

Figure 14: Articular cartilage formations and endochondral cartilage formations in bone marrow (Solochrome stain). **A.** Endochondral cartilage formations with two cartilage cells columns, areas of hypertrophic cells (red arrows) and cartilage/bone junction (blue arrows) (Scale bar 40 µm). **B.** Endochondral cartilage formations with three cartilage cells columns, proliferative area (yellow arrow), hypertrophic cells area (red arrow) with cartilage/bone junction (blue arrow) (Scale bar 40 µm). **C.** Endochondral cartilage formation (arrow), less favorably oriented section, nevertheless hypertrophic cells area is recognizable (Scale bar 50µm). **D.** For comparison with fig A and B, view of the native growth plate in the same sample comprising columns of proliferative cells (yellow arrow), hypertrophic cells area (red arrow) and cartilage/bone junction (blue arrow) (Scale bar 40 µm). **E** Articular cartilage/subchondral bone formation, radial layer of cartilage (green arrow), sub-chondral bone (orange arrows) (Scale bar 40 µm). **F.** Articular cartilage/subchondral bone formation, radial layer of cartilage (green arrow), cartilage/bone junction (orange arrow) and tide mark (light green arrow) (Scale bar 40 µm). **G.** Articular cartilage/subchondral bone formation, the low part of radial layer is visible with cartilage/subchondral junction (orange arrow) and tide mark (light green arrow) (Scale bar 20 µm). **H.** For comparison with figures E,F,G view of articular cartilage and subchondral bone in the native articular cartilage of the same sample showing radial layer (green arrow, cartilage/subchondral bone junction (orange arrows)and tide mark (light green arrow) (Scale bar 40 µm).

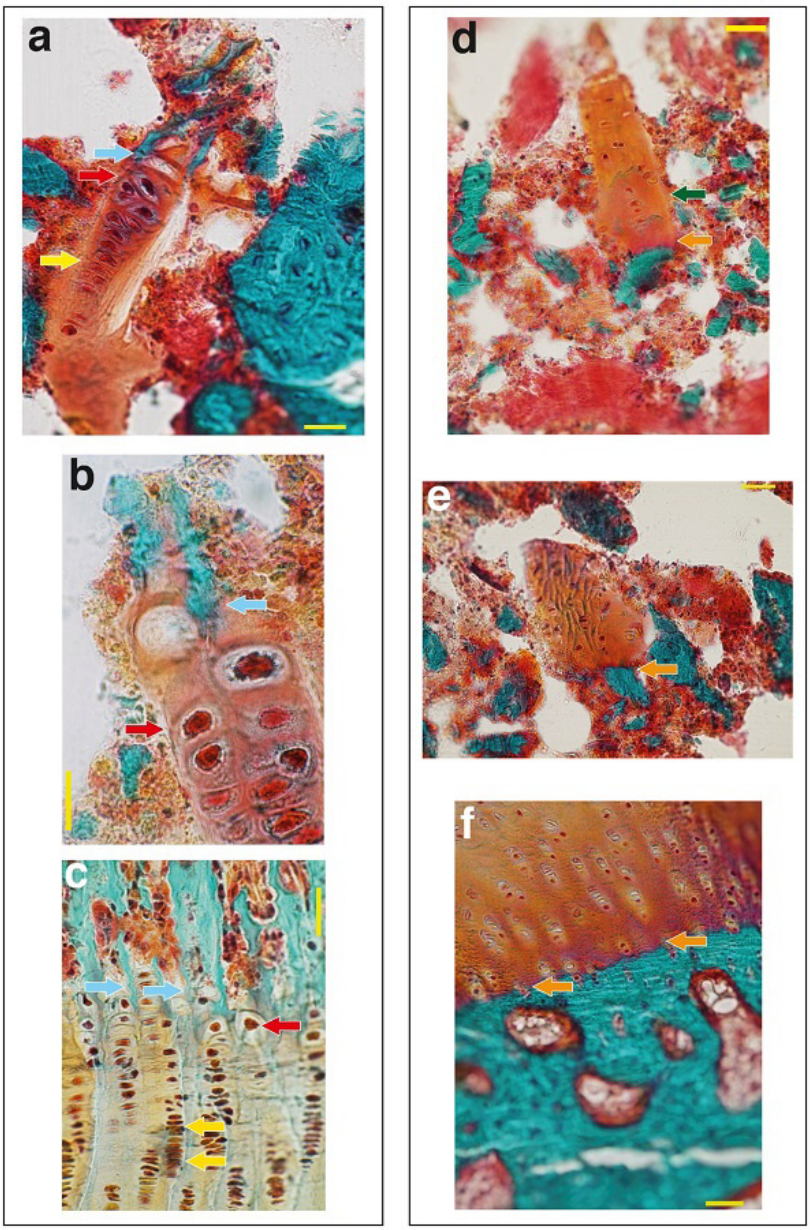

Figure 15: Articular cartilage formations and endochondral cartilage formations in bone marrow (Trichroma stain). **A.** Endochondral cartilage formations with one cartilage cells column, proliferative area (yellow arrow), hypertrophic cells (red arrows) and cartilage/bone junction (blue arrows) (Scale bar 30 µm). **B.** Endochondral cartilage formation, view of the hypertrophic cells area (red arrow) and cartilage/bone junction (blue arrow) (Scale bar 20 µm). **C.** For comparison with fig A and B, view of the native growth plate in the same sample comprising columns of proliferative cells (yellow arrows), hypertrophic cells area (red arrow) and cartilage/bone junction (blue arrows) (Scale bar 40 µm). **D**. Articular cartilage/subchondral bone formation, radial layer of cartilage (green arrow) and cartilage/bone junction (Scale bar 40 µm). **E.** Articular cartilage/subchondral bone formation with cartilage/bone junction (orange arrow) (Scale bar 40 µm). **F.** For comparison with figures E,F view of articular cartilage and subchondral bone in the native articular cartilage of the same sample showing cartilage/subchondral bone junction (orange arrows) (Scale bar 40 µm).

Discussion

General considerations

The main finding of our earlier work was that periosteum flaps can generate significant volumes of bone tissue. We observed in the periosteum grafts sites the formation of osteocartilaginous tissues following a sequence of events involving the constitution of a cartilage anlage, the development of an ossification front, resulting in the replacement of cartilage by bone, then the remodeling of bone with formation of a medulla. This sequence of events, which corresponds to a typical developmental endochondral ossification process has already been described in periosteal flap models [6,11]. It also corresponds to how a bone fracture callus normally forms. Nevertheless, in the articular model, this development sequence was influenced by movement with transient persistence of patches of endochondral cartilage in regions subject to movements. The preliminary work published by this paper's authors may be consulted for mechanobiology considerations [10]. Furthermore, intense bone remodeling in underlying native's bones beneath the periosteal graft and necrosis in adjacent skeletal muscle were observed in the early stage. Nevertheless, it's the presence of connective tissue cells collections in bone marrow and the tissue spaces surrounding the periosteum graft which requires comments and will be the main topic of this discussion.

Activation/differentiation of progenitor cells

The cells observed in cells collections correspond to the basic elements of the tissues from which limbs are formed, i.e. bone, skeletal muscle, cartilage, but they accumulate in an anarchic fashion. Bone cell formations account for most of the structures seen with cartilaginous and muscle formations in the minority. Nor was any specific distribution in space observed for cartilaginous or muscle cells within these various cell collections. The presence of these collections appears to be governed by a process of recruitment and differentiation of skeletal progenitor cells with the diffusion of soluble factors from the periosteum graft to the surrounding tissues impacting skeletal progenitor cells. The first steps of the process are well visible in stage D4 of the articular model observation which also suggests the existence of a proliferative step in the bone marrow, while mature bone and cartilage cells are already present in the joint cavity and muscles. Local resident bone marrow progenitor cells can be the cell source in the bone marrow [1,2,12] and synovial membrane progenitors for the cells identified in joint cavities [13-15]. Skeletal muscle interstitial connective tissue could be the source of progenitors cells in the intermuscular septa [16,17]. The involvement of circulating cells is also possible in all these compartments [18-20].

In bone marrow, cell collections were observed to be highly variable in density, some containing none or very few cells and others being richer in cells. This is consistent with the results of a study that reported high variability in marrow-derived skeletal progenitor's cells content in rabbits, with a coefficient of variation of 77 between different preparations [21]. This great inter-individual variability made it difficult to take a quantitative approach to the phenomena observed in our work. With respect to intra-articular and intra-muscular cells showing signs of cell injury, unlike in bone marrow such cells are submitted to mechanical constraints in these two areas. Unusually, we could observe well preserved intra-articular cartilage formations (Figure 13C).

It is possible that cell collections in muscles and joint spaces could be due to "contamination" by progenitor cells coming from the periosteum. However, by virtue of their compact microarchitecture, cortical bone and blocks of articular cartilage constitute *a priori* a physical barrier to contamination by cells passing from a flap's implantation zone into the bone marrow. On this issue, let us remember that the surgical procedure did not create breaking in the cortical bone. In addition, the bone remodeling visible at D4 does not seem to lead to breaking intrusion of the cortical bone. Nevertheless, with a view to confirming that it is indeed the activation of local progenitor cells rather than periosteum cells contamination of bone marrow which operates, we conducted an extra experiment: a periosteal flap was harvested in the same way and directly repositioned on the tibia with a semipermeable filter (pore size 0.4 µm) which blocked cell migration but allowed soluble factors to pass. Bone cell formations were observed in the underlying tibia local bone marrow (Figure 7F).

Which soluble factors are involved?

In terms of the soluble factors that could be involved in the process, it should be noted that the periosteum secretes significant amounts of IL-6, IL-8, GM-CSF and TGF-beta [22]. Bone morphogenetic proteins are also produced at an early stage by periosteal explants [23,24]. Such factors induce bone marrow mesenchymal stem cells to undergo osteogenic differentiation [25]. Circulating bone marrow-derived osseous progenitors are recruited in bone-forming sites by the CXCR4/Stromal cell-Derived Factor-1 (SDF-1) pathway [26,27]. Moreover, SDF-1 is induced in the periosteum of injured bone and appears to promote endochondral bone repair by recruiting mesenchymal stem cells to the site of injury [28]. TGF-beta is a key factor for chondrogenic differentiation of mesenchymal stem cells [29]. The same soluble factors are described in molecular profiling of fractures [30]. It should be noted that periosteum grafts typically affect only bone and cartilage differentiation pathways. This is why it may be suggested that the concomitant muscle necrosis/regeneration process observed in adjacent skeletal muscles is responsible for the recruitment of the skeletal muscle progenitors present in the bone marrow, through the diffusion of soluble factors from regenerating skeletal muscle. Nonetheless, it is possible that skeletal muscle progenitor cells are also activated by soluble factors given off

directly by the periosteum graft, but our findings do not enable us to solve this question.

Two very different types of cartilage

The most important aspect, however, is the demonstration of cartilage progenitors undergoing differentiation via the endochondral pathway while others are differentiated via the articular pathway. Both types were observed in bone marrow whereas only endochondral cartilage was clearly seen in the joint space and muscles although, given the difficulties of making observations in these cell collections that are less well preserved in these types of space, this does not necessarily mean that articular cartilage was absent. Everything seems to indicate that two distinct types of cartilage progenitors coexist in the bone marrow, first progenitors of the endochondral pathway (which -*stricto sensu*- could be called "endochondral pathway bone progenitor cells" instead of cartilage progenitors) and secondly, specific articular cartilage progenitor cells. These last cells produce formations with a full articular cartilage architecture that escape the hypertrophic phenotype of the endochondral pathway. In parallel, specific endochondral progenitors are also activated and produce formations with a characteristic endochondral ossification architecture. This is an important point because, while the hypertrophic phenotype constitutes the default differentiation pathway of mesenchymal stem/progenitor cells for cartilage formation, escaping the endochondral pathway is a key component of cartilage tissue engineering to produce permanent articular cartilage. Authors consider in a cartilage repair perspective (tissue engineering) that maintaining a stable, prehypertrophic cellular phenotype is essential for the long-term stability of cartilage [31]. While the use of bone marrow mesenchymal stem cells is currently an active line of research, numerous protocols for regenerating articular cartilage that use them do not perfectly restore hyaline cartilage which leads to the appearance of fibro-hypertrophic cartilage [32]. That is why blocking the appearance of a hypertrophic phenotype and cartilage "shape retention" of tissue engineered cartilage is currently a very active line of research [33-36]. Note that conversely, the hypertrophic phenotype of cartilage is sought after for bone production from stem cells having entered the endochondral pathway [37]. The existence of two distinct cartilaginous progenitor subtypes may be related to the fact that articular cartilage differs substantially from endochondral cartilage through different chondrogenic early developmental fates. One fate leads to transient cartilage, during skeletal development (or fracture repair), which will disappear with skeletal maturation while the other will lead to cartilage that lasts throughout a lifetime [38]. This contradicts the traditional view, which considers articular cartilage as representing a part of cartilage anlage that is not replaced by bone through endochondral ossification. In particular, cells present at prospective joint sites (interzone) in developing limbs and expressing the growth differentiation factor 5 (GDF5) gene, constitute a distinct cohort of progenitor cells responsible for limb joint formation, including articular cartilage, with no contribution to adjacent cartilage diaphysis and growth plate formation [39]. These two distinctive fates are also reflected early in development in the different compositions of their respective extracellular matrix [40].

A full, integrated program of phenotypic development into articular cartilage

Another aspect that should be highlighted is that of the micro-architecture of articular cartilage micro formations observed in bone marrow. This architecture is completely identical to that of normal articular cartilage, with radial (deep), transitional (middle) and tangential (superficial) layers. Let us remember that the histologic appearance of these three different layers is consistent with the functional complexity of articular cartilage. In our observations, this special architecture appears to be the result of an integrated development process that starts with activation of a preprogrammed articular cartilage progenitor cell.

It is known that bone marrow skeletal progenitors can form a cartilage-like tissue *in vitro* under the guidance of specific cocktails of growth factors. The resulting differentiated tissue can be classified as cartilage in that it expresses many biomolecules typical of hyaline cartilage, such as type II collagen and the proteoglycan, aggrecan. However, the proportions of these chemical constituents is unsatisfactory in these tissue engineered cartilage. Also the stratified ultrastructure and spatial organization of native cartilage are completely absent, resulting in poor mechanical properties [31].

Let's remember that natural articular cartilage has a stratified ultrastructure with biochemical composition and biophysical properties specific to each of its layers. Although the cartilage contains only a single type of cell referred to as chondrocytes, the cells in different layers have distinct morphologies and functionalities [41]. Each articular cartilage layer has a distinct matrix composition, local oxygen tension, and biomechanical capacities. Superficial zone chondrocytes (tangential layer) are flattened and secrete surface zone protein, a proteoglycan that decreases the friction between the two articular plates. The middle zone is characterized by a seemingly random fibrillar structure and matrix producing chondrocytes. The deep zone consists of large diameter collagen fibrils oriented perpendicularly to the articular surface with chondrocytes which tend to arrange themselves in columns.

Furthermore, the cartilage formations observed in the marrow are free of mechanical stress, they "float" freely in the marrow fat. The microarchitecture of articular cartilage may therefore be independent of the mechanical context as suggested by studies proposing that the various specific layers of articular cartilage

are the result of "functional histomorphology" corresponding to modelling by the mechanobiologic context [42]. Some studies suggesting notably that the presence of flattened cells in the tangential layer of articular cartilage is the result of tangential strains [43].

Similarly, it is also interesting to note that in the articular cartilage formations, we frequently observed an additional bony component with a cartilage/ subchondral bone junction suggesting that both the cartilaginous and the bone components develop from the same progenitors. Such observation suggests that this bone component in osteocartilaginous formations is also part of an integrated program of phenotypic development which seems to dictate both the fine architecture of the cartilaginous component and the presence of subchondral bone. This agrees well with observations in a recent study conducted in a juvenile mouse model. This showed that cells in the superficial layer of articular cartilage produce all cartilage [44]. In this construction, the bone component would be provided by a process of cartilaginous cell trans differentiation [45,46]. Furthermore, these different observations may be also related to the concept of articular cartilage-subchondral bone units in normal and pathologic articular cartilage, suggesting unity between the cartilaginous and bony aspects of the so called osteochondral unit [47-49].

Concluding Remarks

Tissue engineering with which "raw material"?

Repairing articular cartilage remains a major challenge [50,51], and is a focus of intense research. Tissue engineering is an essential aspect of innovative techniques to produce long-lasting cartilage. The "raw material" for tissue engineering are populations of MSCs [1,2]. However, what is currently termed MSCs is not a homogeneous population of cells, which affect the ability to obtain optimal results in cartilage tissue engineering. The identity and localization of articular cartilage progenitor cells remains studying, some authors doubt its existence [31]. As already pointed out, in the tissue engineering of articular cartilage, the endochondral pathway (hypertrophic phenotype) constitutes the default differentiation pathway of MSCs for cartilage formation leading to transient cartilage formation. Some try to prevent the appearance of hypertrophic cellular phenotype. Extremely complex techniques are also being developed to artificially generate a functionally integrated, stratified cartilage-bone structure (multiphasic osteochondral tissue engineering), for example with "biomimetic" multi-phasic scaffolds [52-55].

Nevertheless, our work shows that among MSCs, some cells have an intrinsic ability to differentiate specifically into articular cartilage, leading to the formation of tissues micro complexes including all the layers of this tissue.

With respect to tissue engineering, our observations support the development of research protocols that select the proper population of articular cartilage progenitors before its use as cartilage building units.

Acknowledgements

This work was supported by grants from *Fondation de L'Avenir* and the newspaper *Midi-Libre*. We are grateful to P Clézardin, D Farlay and A.M Buffet (INSERM U 831 Lyon), R Niemenchiesky and H Taillades (Experimental Surgery Laboratory, School of Medicine, Montpellier I University) for their technical assistance.

Author Contributions

All the authors contributed equally to this work.

References

1. Arthur A, Zannettino A, Gronthos S (2009) The therapeutic applications of multipotential mesenchymal/stromal stem cells in skeletal tissue repair. J Cell Physiol 218: 237-245.
2. Berebichez-Fridman R, Gómez-García R, Granados-Montiel J, Berebichez-Fastlicht E, Olivos-Meza A, et al. (2017) The holy grail of orthopedic surgery: Mesenchymal stem cells-their current uses and potential applications. Stem Cells Int 2017: 2638305.
3. Malizos KN, Papatheodorou LK (2005) The healing potential of the periosteum molecular aspects. Injury 36: S13-S19.
4. Colnot C, Zhang X, Knothe Tate ML (2012) Current insights on the regenerative potential of the periosteum: molecular, cellular, and endogenous engineering approaches. J Orthop Res 30: 1869-1878.
5. Duchamp de Lageneste O, Julien A, Abou-Khalil R, Frangi G, Carvalho C, et al. (2018) Periosteum contains skeletal stem cells with high bone regenerative potential controlled by Periostin. Nat Commun 9: 773.
6. Poussa M, Ritsila V (1979) The osteogenic capacity of free periosteal and osteoperiosteal grafts. a comparative study in growing rabbits. Acta Orthop Scand 50: 491-499.
7. Ritsilä VA, Santavirta S, Alhopuro S, Poussa M, Jaroma H, et al. (1994) Periosteal and perichondral grafting in reconstructive surgery. Clin Orthop Relat Res 302: 259-265.
8. Zarnett, R, Salter RB (1989) Periosteal neochondrogenesis for biologically resurfacing joints: its cellular origin. Can J Surg 32: 171-174.
9. van der Meulen MC, Huiskes R (2002) Why mechanobiology? A survey article. J Biomech 35: 401-414.
10. Moukoko, D, Pourquier, D, Pithioux M, Chabrand P (2010) Influence of cyclic bending loading on *in vivo* skeletal tissue regeneration from periosteal origin. Orthop Traumatol Surg Res 96: 833-839.
11. Ueno T, Kagawa T, Fukunaga J, Mizukawa N, Kanou M, et al. (2003) Regeneration of the mandibular head from grafted periosteum. Ann Plast Surg 51: 77-83.
12. Pittenger MF, Mackay AM, Beck SC, Jaiswal RK, Douglas R, et al. (1999) Multilineage potential of adult human mesenchymal stem cells. Science 284: 143-147.

13. Jones BA, Pei M (2012) Synovium-derived stem cells: a tissue-specific stem cell for cartilage engineering and regeneration. Tissue Eng Part B Rev 18: 301-311.

14. De Bari BC, Dell'Accio F, Tylzanowski P, Luyten FP (2001) Multipotent mesenchymal stem cells from adult human synovial membrane. Arthritis Rheum 44: 1928-1942.

15. de Sousa EB, Casado PL, Moura Neto V, Duarte ME, Aguiar DP (2014) Synovial fluid and synovial membrane mesenchymal stem cells: latest discoveries and therapeutic perspectives. Stem Cell Res Ther 5: 112.

16. Jackson WM, Lozito TP, Djouad F, Kuhn NZ, Nesti LJ, et al. (2011) Differentiation and regeneration potential of mesenchymal progenitor cells derived from traumatized muscle tissue. J Cell Mol Med 15: 2377-2388.

17. Young HE (2001) Human reserve pluripotent mesenchymal stem cells are present in the connective tissues of skeletal muscle and dermis derived from fetal, adult, and geriatric donors. Anat Rec 264: 51-62.

18. Eghbali-Fatourechi GZ, Lamsam J, Fraser D, Nagel D, Riggs BL, et al. (2005) Osteoblast-lineage cells in humans. N Engl J Med 352: 1959-1966.

19. Huss R, Lange C, Weissinger EM, Kolb HJ, Thalmeier K (2000) Evidence of peripheral blood-derived, plastic-adherent CD34(-/low) hematopoietic stem cell clones with mesenchymal stem cell characteristics. Stem Cells 18: 252-260.

20. Wang SJ, Yin MH, Jiang D, Zhang ZZ, Qi YS, et al. (2016) The Chondrogenic Potential of Progenitor Cells Derived from Peripheral Blood: A Systematic Review. Stem Cells Dev 25: 1195-1207.

21. Solchaga LA, Johnstone B, Yoo JU, Goldberg VM, Caplan AI (1999) High variability in rabbit bone marrow-derived mesenchymal cell preparations. Cell Transplant 8: 511-519.

22. Brittberg M, Sjögren-Jansson E, Thornemo M, Faber B, Tarkowski A, et al. (2005) Clonal growth of human articular cartilage and the functional role of the periosteum in chondrogenesis. Osteoarthritis Cartilage 13: 146-153.

23. Sanyal A, Sarkar G, Saris DB, Fitzsimmons JS, Bolander ME, et al. (1999) Initial evidence for the involvement of bone morphogenetic protein-2 early during periosteal chondrogenesis. J Orthop Res 17: 926-934.

24. O'Driscoll SW (1999) Articular cartilage regeneration using periosteum. Clin Orthop Relat Res 367: S186-S203.

25. Luu HH, Song WX, Luo X, Manning D, Luo J, et al. (2007) Distinct roles of bone morphogenetic proteins in osteogenic differentiation of mesenchymal stem cells. J Orthop Res 25: 665-677.

26. Otsuru S, Tamai K, Yamazaki T, Yoshikawa H, Kaneda Y (2008) Circulating bone marrow-derived osteoblast progenitor cells are recruited to the bone-forming site by the CXCR4/stromal cell-derived factor-1 pathway. Stem Cells 26: 223-234.

27. Shinohara K, Greenfield S, Pan H, Vasanji A, Kumagai K, et al. (2011) Stromal cell-derived factor-1 and monocyte chemotactic protein-3 improve recruitment of osteogenic cells into sites of musculoskeletal repair. J Orthop Res 29: 1064-1069.

28. Kitaori T, Ito H, Schwarz EM, Tsutsumi R, Yoshitomi H, et al. (2009) Stromal cell-derived factor 1/CXCR4 signaling is critical for the recruitment of mesenchymal stem cells to the fracture site during skeletal repair in a mouse model. Arthritis Rheum 60: 813-823.

29. Weiss S, Hennig T, Bock R, Steck E, Richter W (2010) Impact of growth factors and PTHrP on early and late chondrogenic differentiation of human mesenchymal stem cells. J Cell Physiol 223: 84-93.

30. Villafan-Bernal JR, Franco-De La Torre L, Sandoval-Rodriguez AS, Armendariz-Borunda J, Alcala-Zermeno JL, et al. (2016) Molecular profiling of a simple rat model of open tibial fractures with hematoma and periosteum disruption. Exp Ther Med 12: 3261-3267.

31. Somoza RA, Welter JF, Correa D, Caplan AI (2014) Chondrogenic differentiation of mesenchymal stem cells: challenges and unfulfilled expectations. Tissue Eng Part B Rev 20: 596-608.

32. Baugé C, Boumédiene K (2015) Use of adult stem cells for cartilage tissue engineering: current status and future developments. Stem Cells Int 2015: 438026.

33. Chen S, Fu P, Cong R, Wu H, Pei M (2015) Strategies to minimize hypertrophy in cartilage engineering and regeneration. Genes Dis 2: 76-95.

34. Tang X, Fan L, Pei M, Zeng L, Ge Z (2015) Evolving concepts of chondrogenic differentiation: history, state-of-the-art and future perspectives. Eur Cell Mater 30: 12-27.

35. Choi SM, Lee KM, Ryu SB, Park YJ, Hwang YG, et al. (2018) Enhanced articular cartilage regeneration with SIRT1-activated MSCs using gelatin-based hydrogel. Cell Death Dis 9: 866.

36. Inaki R, Fujihara Y, Kudo A, Misawa M, Hikita A, et al. (2018) Periostin contributes to the maturation and shape retention of tissue-engineered cartilage. Sci Rep 8: 11210.

37. Scotti C, Piccinini E, Takizawa H, Todorov A, Bourgine P, et al. (2013) Engineering of a functional bone organ through endochondral ossification. Proc Natl Acad Sci USA 110: 3997-4002.

38. Moskalewski S, Hyc A, Jankowska-Steifer E, Osiecka-Iwan A (2013) Formation of synovial joints and articular cartilage. Folia Morphol (Warsz) 72: 181-187.

39. Koyama E, Shibukawa Y, Nagayama M, Sugito H, Young B, et al. (2008) A distinct cohort of progenitor cells participates in synovial joint and articular cartilage formation during mouse limb skeletogenesis. Dev Biol 316: 62-73.

40. Gregory KE, Keene DR, Tufa SF, Lunstrum GP, Morris NP (2013) Developmental distribution of collagen type XII in cartilage: association with articular cartilage and the growth plate. J Bone Miner Res 16: 2005-2016.

41. Yin L, Wu Y, Yang Z, Denslin V, Ren X, et al. (2018) Characterization and application of size-sorted zonal chondrocytes for articular cartilage regeneration. Biomaterials 165: 66-78.

42. Wong M, Carter DR (2003) Articular cartilage functional histomorphology and mechanobiology: a research perspective. Bone 33: 1-13.

43. Carter DR, Wong M (2003) Modelling cartilage mechanobiology. Philos Trans R Soc Lond B Biol Sci 358: 1461-147.

44. Li L, Newton PT, Bouderlique T, Sejnohova M, Zikmund T, et al. (2017) Superficial cells are self-renewing chondrocyte progenitors, which form the articular cartilage in juvenile mice. FASEB J 31: 1067-1084.

45. Wolff LI, Hartmann C (2019) A Second Career for Chondrocytes-Transformation into Osteoblasts. Curr Osteoporos Rep 17: 129-137.

46. Yang L, Tsang KY, Tang HC, Chan D, Cheah KS (2014) Hypertrophic chondrocytes can become osteoblasts and osteocytes in endochondral bone formation. Proc Natl Acad Sci U S A 111: 12097-12102.

47. Funck-Brentano T, Cohen-Solal M (2011) Crosstalk between cartilage and bone: when bone cytokines matter. Cytokine Growth Factor Rev 22: 91-97.

48. Findlay DM, Atkins GJ (2014) Osteoblast-chondrocyte interactions in osteoarthritis. Curr Osteoporos Rep 12: 127-134.

49. Orth P, Cucchiarini M, Kohn D, Madry H (2013) Alterations of the subchondral bone in osteochondral repair-translational data and clinical evidence. Eur Cell Mater 25: 299-316.

50. Huey DJ, Hu JC, Athanasiou KA (2012) Unlike bone, cartilage regeneration remains elusive. Science 338: 917-921.

51. Tuan RS, Chen AF, Klatt BA (2013) Cartilage regeneration. J Am Acad Orthop Surg 21: 303-311.

52. Gadjanski I, Vunjak-Novakovic G (2014) Challenges in engineering osteochondral tissue grafts with hierarchical structures. Expert Opin Biol Ther 15: 1583-1599.

53. Longley R, Ferreira AM, Gentile P (2018) Recent approaches to the manufacturing of biomimetic multi-phasic scaffolds for osteochondral regeneration. Int J Mol Sci 19: E1755.

54. Jeon JE, Vaquette C, Klein TJ, Hutmacher DW (2014) Perspectives in multiphasic osteochondral tissue engineering. Anat Rec (Hoboken) 297: 26-35.

55. Correia CR, Reis RL, Mano JF (2015) Multiphasic, multistructured and hierarchical strategies for cartilage regeneration. Adv Exp Med Biol 881: 143-160.